Supporting Information

Thurley and Falcke 10.1073/pnas.1008435108

SI Text

The supporting information contains the following:

1. Details of the computation of Ca^{2+} diffusion profiles and opening transition times from single-channel models, which are required as input data to the model described in the main text.
2. Full analytic treatment of the model in terms of intergral equations.
3. A direct stationary solution of the model in the special case of a tetrahedral arrangement of channel clusters.
4. A delayed stochastic simulation algorithm suitable for Monte Carlo simulations of the model.
5. Details of the implementation of a global feedback
6. The σ–T_{av} relation and biological function
7. Opening transition probabilities ψ_o at different Ca^{2+} concentration profiles (Fig. S1).
8. Solutions of the full, time-dependent model obtained by numerical integration of the integral equations (Fig. S2).
9. Comparative stochastic simulations of the cube model and the tetrahedron model (Fig. S3).
10. A schematic caricature of responses to stimulation in the σ–T_{av} plot (Fig. S4).
11. Simulations of Ca^{2+} currents due to open clusters, which demonstrate that cluster coupling strength can be well approximated by a time-independent value during a puff (Fig. S5).
12. Spiking conditions at different numbers of channels per cluster, showing that these shift the curves only slightly at realistic values of the channel closing rate (Fig. S6).
13. Parameter values of the De Young–Keizer model used to compute the opening transition probabilities ψ_o (Table S1).
14. A comparison of the different methods to solve the model equations (Table S2).

Ca^{2+} Diffusion and Opening Transition Times. As input data to our hierarchic stochastic model, we need details of the cluster coupling by Ca^{2+} and of the probability densities for cluster opening and closing. In *Methods* of the main text, we derived the closing probability $\psi_c(t-\tau)$ (Eq. **S2**) and gave a general description of the opening probabilities $\psi_o(c,t-\tau)$ and of our Ca^{2+} diffusion model. The details will be provided here.

Ca^{2+} diffusion profile. In the main text, we argued that Ca^{2+} dynamics can be described by point sources at the locations of open channel clusters, diffusion in the cytosol, and constant activity of Ca^{2+} pumps. Therefore, the Ca^{2+} concentration is governed by a linear reaction–diffusion equation:

$$\frac{\partial}{\partial t}[\mathrm{Ca}^{2+}](r,t) = D\Delta[\mathrm{Ca}^{2+}] + \rho \sum_{\substack{n=1 \\ r\neq r_n}}^{N_o} \delta(r-r_n) - p[\mathrm{Ca}^{2+}], \qquad \textbf{[S1]}$$

where D is the Ca^{2+} diffusion coefficient; ρ is the average Ca^{2+} current through a cluster; p is the rate at which Ca^{2+} is pumped out of the cytosol by Ca^{2+} pumps (called SERCAs); the vector r is the spatial coordinate; r_n is the position of cluster n; $\delta(r)$ and Δ are the Dirac δ-function and the Laplacian in three dimensions, respectively; and the sum runs over all N_o open clusters.

Further, in the main text, we justified the use of stationary Ca^{2+} concentration profiles, in which the Ca^{2+} current ρ corresponds to the average current through an open cluster. With free boundary conditions (i.e. $\lim_{r\to\infty}[\mathrm{Ca}^{2+}] = 0$), and if we take into account the continuous presence of a resting Ca^{2+} concentration c_0, the stationary solution to Eq. **S1** at closed clusters c_m is (1)

$$c_m = \frac{\rho}{D}\sum_{\substack{n=1 \\ n\neq m}}^{N_o} \frac{e^{-\sqrt{\frac{p}{D}}|r_m-r_n|}}{4\pi|r_m-r_n|} + c_0. \qquad \textbf{[S2]}$$

Ca^{2+} diffusion profiles computed from Eq. **S2** are shown in Fig. S1*A*. More general boundary conditions leading to more complex Ca^{2+} diffusion profiles can be used instead of Eq. **S2** without difficulty for what follows.

In Table 1, we provide the value of the release current of the IP_3R in units of picoamperes, but it is required in units of micromoles per second for Eqs. **S1** and **S2**. We estimated the value in units of micromoles per second as follows: By Faraday's law, $\rho = I/(zF) \approx 10^{-12}\ \mu\mathrm{mol\,s^{-1}}$, if I is the release current of 0.2 pA given in Table 1, $z = 2$ is the valency of Ca^{2+} ions, and $F \approx 10^5\,\mathrm{As\,mol^{-1}}$ is Faraday's constant. However, the 3D δ-function multiplied to ρ in Eq. **S1** has dimension $\mu\mathrm{m}^{-3}$, whereas the left-hand side has dimension $(\mu\mathrm{M\,s})^{-1}$, so that by the transformation from liter to cubic micrometer a factor of 10^{15} enters ρ. Further, we assume that on average three channels are open during a puff, and we end up with $\rho = 3000\ \mu\mathrm{mol\,s^{-1}}$, which we use in simulations.

Opening transition times. The opening probability densities $\psi_o(c,t-\tau)$ introduced in the main text depend on the local Ca^{2+} and IP_3 concentrations as well as on the number of channels in the cluster N_{ch}. We index only the Ca^{2+} concentration c, because it depends on the configuration (see below) and therefore drives the spatiotemporal dynamics. ψ_o and ψ_c can be measured, and indeed we use the measured closing time distribution given by Eq. **2** in the main text. But because ψ_o has only been measured for resting $[Ca^{2+}]$, and not for a range of concentrations yet, we calculate it from models as described in the following.

Opening transition times are obtained from the method developed by Higgins et al (2). The method uses the De Young–Keizer model (3) for the description of the individual IP_3Rs with the parameter values given in Table S1. On the basis of that model, ψ_o can be computed from the master equation describing the random channel state changes. Briefly, the De Young–Keizer model assumes that a channel is open when three out of the four subunits of the IP_3R are bound by IP_3 and activating Ca^{2+}, but not by inhibiting Ca^{2+}. The transition rates between the states could be determined by experiments to some extent.

Because the probability densities obtained that way are sums of >1000 exponentials, making computation of function values rather extensive, we sought for a simpler expression of ψ_o that is more suitable for efficiently solving the system. A useful assumption for the analysis of waiting times is that they can be described by the two-parametric γ-distribution

$$\psi_o(c,\theta) = \frac{\theta^{\alpha(c)-1}e^{-\theta/\beta(c)}}{\Gamma(\alpha(c))\beta(c)^{\alpha(c)}}, \qquad \textbf{[S3]}$$

where $\theta = t-\tau$, $\Gamma(x)$ is the Euler Γ function, α is the shape parameter, and β is the scale parameter. If α is an integer, the γ-distribution describes the probability density for the αth Poisson event with rate $1/\beta$ in a process consisting of α subsequent Poisson processes. Because within a cluster many independent state transitions of individual clusters can occur before an open

cluster configuration is achieved, this is a realistic model for our purposes.

For $\alpha = 1$, the γ-distribution is equal to the exponential distribution describing a Markovian rate process:

$$\psi_o(c,\theta) = \lambda(c)e^{-\lambda(c)\theta}, \qquad \lambda(c) = \frac{1}{\beta(c)}. \qquad \textbf{[S4]}$$

Fig. S1 shows the ψ_o computed from the De Young–Keizer model for diffusion profiles computed according to Eq. **S2**. The computed ψ_o fit Eq. **S3** well at high values of $[Ca^{2+}]$, which are expected during a spike, whereas at resting $[Ca^{2+}]$, ψ_o better fits Eq. **S4**. Therefore, we fit the probability distribution for opening of the first cluster by Eq. **S4** and refer to the parameter λ (or λ_0; compare *Implementation of the Global Feedback*) as the puff rate (Table 1).

Formulation of the Hierachic Stochastic Model in Terms of Integral Equations. The system variables of the hierarchic stochastic model of intracellular Ca^{2+} dynamics, in their most general form, are solutions of a set of Volterra integral equations (VIEs), which will be derived in this section. The procedure is a generalization of the formalism developed by Prager et al. to more states and state transitions (4).

Non-Markovian master equation. The state of the cell is described by the configuration of open and closed clusters among its N_{cl} clusters. To formulate these ideas mathematically, we introduce the state variable x_j for all clusters $j = 1,\ldots,N_{cl}$, which can assume the values O or C. The set of all possible configurations of open and closed clusters is denoted $S_i = \{x_1^i,\ldots x_{N_{cl}}^i\}$, $i = 0,\ldots,N_{conf}$, where N_{conf} is the number of configurations with at least one open cluster, and $x_j^i \in \{O,C\}$.

We denote with $c_j(S_i)$ the Ca^{2+} concentration at cluster j in configuration S_i. Then, the stationary solution to our diffusion problem Eq. **S2** becomes

$$c_m(S_i) = \frac{\rho}{D}\sum_{\substack{n=1\\ n\neq m}}^{N_o} \frac{e^{-\sqrt{\frac{p}{D}}|r_m - r_n|}}{4\pi|r_m - r_n|} + c(S_0), \qquad \textbf{[S5]}$$

where S_0 is the configuration with all channels closed and $c(S_0) = c_0$ is the resting Ca^{2+} concentration. The probability $P(S_i,t)$ to be in configuration S_i at time t obeys the master equation

$$\frac{\partial}{\partial t}P(S_i,t) = \sum_{\substack{l=0\\ l\neq i}}^{N_{conf}} I_{li}(\{c_j(S_i)\},t) - I_{il}(\{c_j(S_i)\},t), \qquad \textbf{[S6]}$$

with the probability fluxes I_{il} for a transition from S_i to S_l, and where braces $\{\cdot\}$ indicate dependence on all clusters j.

In the case of a Markovian rate process, each transition would only depend on the configuration at the last time step, and we would be able to write

$$I_{il}(\{c_j(S_i)\},t) = r_{il}(\{c_j(S_i)\},t)P(S_i,t), \qquad \textbf{[S7]}$$

with transition rates r_{il} determined uniquely by the configuration S_i at time t (5). But, instead of transition rates, the input data to our model are the probability density distributions for opening and closing of clusters, $\psi_o(c,t-\tau)$ and $\psi_c(t-\tau)$ (compare *Methods* in the main text and Ca^{2+} *Diffusion and Opening Transition Times* above). Those depend not only on the configuration at the actual time, but also on the time interval that has passed since the last state change, $t-\tau$. Therefore, the master equation **S6** is non-Markovian, and the problem does not lead to a set of differential equations but requires derivation of integral equations.

To introduce the calculation of the probability fluxes I_{il} in terms of the $\psi_{o,c}$, we first consider the simplest possible setup with only one cluster and two configurations, $S_0 = \{C\}$ and $S_1 = \{O\}$. Then, the I_{il} are solutions of a system of integral equations (4, 6):

$$\begin{pmatrix} I_{01}(t)\\ I_{10}(t)\end{pmatrix} = \int_0^t \begin{pmatrix} 0 & \psi_o(c(S_0),t-\tau)\\ \psi_c(t-\tau) & 0\end{pmatrix}\begin{pmatrix} I_{01}(\tau)\\ I_{10}(\tau)\end{pmatrix}d\tau + \begin{pmatrix} f_{01}(t)\\ f_{10}(t)\end{pmatrix}, \qquad \textbf{[S8]}$$

where we omit dependence of the I_{il} on Ca^{2+} concentrations in configuration S_i, and $f_{il}(t)$ is the initial flux vector (or initial function) containing fluxes from the starting configuration S_i to configuration S_l (see below). An intuitive explanation for this equation can be given as follows: The opening (closing) probability flux at time t is the sum of the initial flux $f_{01}(t)$ ($f_{10}(t)$) and the flux that results from reopening (reclosing). The latter equals the integral over the probabilities to have closed (opened) at earlier times $t-\tau$ multiplied by the probabilities to reopen (reclose) at t.

In general, we consider more than one cluster, and the probability for a transition from configuration S_i to configuration S_l by a state change of cluster j depends on the states of all clusters (or more precisely, on the resulting Ca^{2+} concentration profile). Therefore, we denote the probability distribution for a transition from S_i to S_l by $\psi_{il}(\{c_j(S_i)\},t-\tau)$. The general form of Eq. **S8** then is

$$I_{il}(t) = \int_0^t \psi_{il}(\{c_j(S_i)\},t-\tau)\sum_{\substack{k=0\\ k\neq i}}^{N_{conf}} I_{ki}(\tau)d\tau + f_{il}(t). \qquad \textbf{[S9]}$$

In the remaining part of this section, we denote the time elapsed since the last transition with $\theta = t-\tau$. Then, the configuration transition probability ψ_{il} is given by the transition probability of the jth cluster times the probability that all other clusters remain in their states:

$$\psi_{il}(\{c_j(S_i)\},\theta) = \psi_{o,c}(c_j(S_i),\theta)\times\prod_m\left[1-\int_0^\theta \psi_o(c_m(S_i),t')dt'\right] \times\prod_n\left[1-\int_0^\theta \psi_c(t')dt'\right], \qquad \textbf{[S10]}$$

where m indexes the subset of closed clusters and n indexes the subset of open clusters, both except cluster j. The ψ_{il} are normalized such that

$$\sum_{\substack{i=0\\ i\neq l}}^{N_{conf}}\int_0^\infty \psi_{il}(t')dt' = 1, \qquad \textbf{[S11]}$$

for all configurations S_l, which can be shown by integration by parts. This means that the system does not possess an absorbing state, which is a necessary condition for repetitive spiking.

Solvability and initial conditions. The integral equation **S9** belongs to the class of VIEs with convolution kernels (7). In contrast to differential equations, VIEs always possess a unique solution and do not require additional initial values for uniqueness. Nevertheless, the initial properties of VIEs are governed by the function added to their integral part, often called initial function. The trivial solution is always zero: In Eq. **S9**, e.g., $f_{il}(t) = 0 \Rightarrow I_{il}(t) = 0$, regardless of the kernel ψ_{il}.

To determine the correct initial functions for our problem, we start in configuration $S_0 = \{C,\ldots,C\}$, so that all initial fluxes are zero apart from those out of S_0. In the case of one cluster, the

initial condition is $P(S_0,0) = 1$, $P(S_1,0) = 0$, and we have $\psi_{01}(c_j(S_i),\theta) = \psi_o(c_0(S_0),\theta)$, according to Eq. **S10**. The initial function as it appears in Eq. **S8** should describe system dynamics in the absence of reclosing events; i.e., for $I_{10} = 0$. That implies $\theta = t$ and $P(S_0,t) = 1 - \int_0^t \psi_o(t')dt'$. Because $I_{10} = 0$, we infer from Eq. **S9** that

$$f_{01}(t) = -\frac{\partial}{\partial t}P(S_0,t) = \psi_o(t). \qquad \textbf{[S12]}$$

In general, this means

$$P(S_i,0) = 1 \quad \text{and} \quad P(S_k) = 0, \quad \text{with } k \neq i$$
$$\Rightarrow f_{il}(t) = \psi_{il}(\{c_j(S_i)\},t) \quad \text{and} \quad f_{kl}(t) = 0, \quad \text{with } k \neq i. \qquad \textbf{[S13]}$$

The initial functions **S13** complete the mathematical formulation of the model, which provides a unique description of the systems dynamics. A good direct test for the model equations is their reduction to simple cases. For that purpose, assume a Markov process, where the waiting times $\psi_{o,c}$ are exponential distributions $\lambda \exp[-\lambda(t-\tau)]$, with λ depending on the transition type. Then, Eqs. **S9** and **S13** can be transformed to Eq. **S7** by the standard method described in ref. 7.

Calculation of σ and T_{av}. Because spike patterns can be characterized in terms of average (T_{av}) and standard deviation (σ) of interspike intervals (ISIs), we wish to compute these quantities from our model. Fortunately, the ISI distribution is the solution of a well-known first-passage time (FPT) problem: Let $\psi_{\text{FPT}}(S_i,S_l,t)$ denote the probability distribution that S_l is visited for the first time after starting in S_i. Then, the ISI distribution is equal to $\psi_{\text{FPT}}(S_0,S_4,t)$. It can directly be computed from Eqs. **S9** and **S10** (5):

$$P(S_0,S_4,t) = \int_0^t P(S_4,S_4,t-\tau)\psi_{\text{FPT}}(S_0,S_4,\tau)d\tau, \qquad \textbf{[S14]}$$

where $P(S_i,S_j,t)$ is the probability to be in S_j at time t after having started in S_i. Because $P(S_4,S_4,0) = 1$, differentiation yields

$$\psi_{\text{FPT}}(S_0,S_4,t) = \frac{\partial}{\partial t}P(S_0,S_4,t) - \int_0^t \frac{\partial}{\partial t}P(S_4,S_4,t-\tau)\psi_{\text{FPT}}(S_0,S_4,\tau)d\tau. \qquad \textbf{[S15]}$$

This equation belongs to the same class of VIEs as Eq. **S9** and depends merely on $(\partial/\partial t)P(S_0,S_4,t)$, which is already known from Eq. **S6**. Therefore, Eqs. **S6**, **S9**–**S13**, and **S15** form a complete system that uniquely determines spike statistics on the basis of puff characteristics.

Numerical solution for time-dependent spike statistics. Equations **S9**–**S13** define a system of linear VIEs with convolution kernel, which has a unique solution (7). Such equations can often be solved directly by reduction to differential equations or by Laplace transform methods, but this is not possible here because of the rather complicated form of the kernel $\psi(t)$. Therefore, it requires direct numerical integration. We have implemented the integral equations of the tetrahedron model (compare *Stationary Statistics and the Tetrahedron Model*) by the two-step method described by Wolkenfelt (8). For this algorithm, Lubich proved absolute stability (i..e., the numerical solution attains stationarity if the real solution does) for a prototypic system of integral equations (9).

Fig. S2*A* shows a typical solution of the time development of the $P(S_i,t)$, indicating that they rapidly attain stationarity. Solutions for $\psi_{\text{FPT}}(t)$ are depicted in Fig. S2*B*. The probability to spike fast clearly is high if the channel closing probability is low. From $\psi_{\text{FPT}}(t)$, we can easily derive σ and T_{av} as the first and second moments (Table S2). Therefore, we have derived the complete behavior of spike statistics on the basis of a Ca^{2+} diffusion profile and the probability distributions for cluster opening and closing, which can be measured (see main text).

Stationary Statistics and the Tetrahedron Model. Because numerical solution of the integral equations derived in the last section is tedious, we sought to derive direct analytical expressions for steady-state values describing spike statistics. That is useful as a test for the stochastic algorithm described in the next section, and it turns out that many of the results shown in the main text were obtained more efficiently on the basis of the analysis presented here.

The tetrahedron model. We will see below that stationary statistics are particularly easily obtained if transitions between configurations compose a linear chain indexed by the number of open clusters. The only nontrivial realization of that property for our model system is the tetrahedron model depicted in Fig. 2*A* in the main text: Here, all configurations with equal number of open clusters are topologically equivalent, implying that the Ca^{2+} diffusion profile is equal. This is not true for the next easiest configurations, the hexahedron (or cube) and the octahedron.

The time-dependent model equations can be given explicitly in matrix notation as follows:

$$I(t) = \int_0^t \psi(t-\tau)I(\tau)d\tau + f(t), \qquad \textbf{[S16]}$$

with

$$I = \begin{pmatrix} I_{01} \\ I_{10} \\ I_{12} \\ I_{21} \\ I_{23} \\ I_{32} \\ I_{34} \\ I_{43} \end{pmatrix},$$

$$\psi = \begin{pmatrix} 0 & \psi_{01} & 0 & 0 & 0 & 0 & 0 & 0 \\ \psi_{10} & 0 & 0 & \psi_{10} & 0 & 0 & 0 & 0 \\ \psi_{12} & 0 & 0 & \psi_{12} & 0 & 0 & 0 & 0 \\ 0 & 0 & \psi_{21} & 0 & 0 & \psi_{21} & 0 & 0 \\ 0 & 0 & \psi_{23} & 0 & 0 & \psi_{23} & 0 & 0 \\ 0 & 0 & 0 & 0 & \psi_{32} & 0 & 0 & \psi_{32} \\ 0 & 0 & 0 & 0 & \psi_{34} & 0 & 0 & \psi_{34} \\ 0 & 0 & 0 & 0 & 0 & 0 & \psi_{43} & 0 \end{pmatrix}.$$

In this notation, the normalization of $\psi(t)$ (Eq. **S11**) takes the form of a column sum, $\int_0^\infty \sum_x \psi_{xy}(t)dt = 1$, in each column y, where $\psi_{xy}(t)$ is the element in row x and column y of $\psi(t)$.

Direct calculation of the stationary solution. The basic assumption in the forthcoming calculations is that the spike-generating stochastic process is stationary; i.e., $(\partial/\partial t)P(S_i,t) = 0$. Then, from Eq. **S9**,

$$\tilde{I}_{il} = I_{il}(\infty) = C_{il}\sum_{\substack{k=0 \\ k\neq i}}^{N_{\text{conf}}} \tilde{I}_{ki}, \qquad \textbf{[S17]}$$

where $C_{il} = \int_0^\infty \psi_{il}(t')dt'$ is the splitting probability to reach configuration S_l before returning to the ground state S_0 when starting

in S_i. Note that we omit the argument c of the distribution functions in this section for convenience. The $\psi_{il}(\theta)$, $\theta = t - \tau$, were defined in Eq. **S10**. It follows immediately (Eq. **S11**) that $\sum_l C_{il} = 1$.

At this point, one might guess that the solutions of Eq. **S17** will determine the relative number of occurrences of each configuration, leading to

$$\tilde{P}(S_i) = \frac{T_i \sum_{\substack{l=0 \\ l\neq i}}^{N_{\text{conf}}} I_{il}}{\sum_{l=0}^{N_{\text{conf}}} (T_l \sum_{\substack{k=0 \\ k\neq l}}^{N_{\text{conf}}} I_{lk})}, \qquad \textbf{[S18]}$$

where $T_i = \int_0^\infty t' \sum_l \psi_{il}(t')dt'$ is the mean residence time in configuration S_i, and $\tilde{P}(S_i)$ is the stationary sojourn probability. Eq. **S18** is confirmed by Eq. **S24** below and by simulations.

Now, we approach the problem in a different way. If we dealt with a Markov process, the probabilities for state changes would be exponentially distributed with parameters r_{il} (5), and that parameter could be computed from T_i and C_{il}:

$$\psi_{o,c}(\theta) = r_{il} \exp(-r_{il}\theta) \qquad \textbf{[S19]}$$

$$\Rightarrow \psi_{il}(\theta) = r_{il} e^{-\theta \sum_l r_{il}}, \qquad T_i = \frac{1}{\sum_{\substack{l=0 \\ l\neq i}}^{N_{\text{conf}}} r_{il}}, \qquad C_{il} = \frac{r_{il}}{\sum_{\substack{l=0 \\ l\neq i}}^{N_{\text{conf}}} r_{il}} \qquad \textbf{[S20]}$$

$$\Rightarrow \quad r_{il} = \frac{C_{il}}{T_i}. \qquad \textbf{[S21]}$$

Eq. **S20** is a direct consequence of the definitions of T_i and C_{il}, in the case of a Markov process. The expression for T_i is sometimes used as characteristic time of a chemical reaction (10).

To proceed with our non-Markovian process, resume an interesting result from Cox (6) for the alternating renewal process (Eq. **S8**): The stationary probability to be in configuration S_i, $\tilde{P}(S_i)$, does not change if the transition time distribution $\psi_\omega(\theta)$ is replaced by an exponential distribution with the same average transition time. As a generalization, we assume that the stationary statistics of the process with general transition probabilities (as computed in Ca^{2+} *Diffusion and Opening Transition Times*, for example) are equal to those of the Markov process with exponentially distributed transition probabilities. That means, we assume that Eq. **S21** is valid in more general circumstances.

Then, we can apply the theory of birth and death processes in the case of a linear chain $S_0 \rightleftharpoons S_1 \rightleftharpoons \cdots \rightleftharpoons S_{N_{\text{conf}}}$ (5). In particular, for the tetrahedron model with $N_{\text{conf}} = N_{\text{cl}} = 4$, C_{14} is the probability that a puff (S_1) generates a spike (S_4) before all clusters are closed again. It can be expressed in terms of single-step transition probabilities:

$$C_{14} = \frac{C_{12}C_{23}C_{34}}{1 + C_{12}(C_{23} - 1) + C_{23}(C_{34} - 1)}. \qquad \textbf{[S22]}$$

With $[Ca^{2+}]$ at closed clusters below the values causing Ca^{2+}-dependent inhibition, $C_{12} < C_{23} < C_{34} < 1$ applies because of Ca^{2+}-induced Ca^{2+} release. Eq. **S22** shows that $C_{14} \approx C_{12}$ for large C_{12}. In the main text, we identified C_{12} with cluster coupling and derived a general expression for it (Eq. **3**). The finding that $C_{14} \approx C_{12}$ supports this definition in the sense that the probability to open a second cluster C_{12} is also an indicator for spiking. We refer to that in the discussion of spiking conditions in the main text.

$\bar{T}_{av}$ and $\bar{\sigma}$ are, in fact, moments of the FPT to go from S_0 to S_4 and can be obtained from recursion relations derived by Gillespie (11), as well as the stationary probabilities. The relations for $\bar{T}_{\text{av}}$ and $\bar{P}(S_0)$ are rewritten as analytic formulas in terms of model variables by simple algebra (the others are too long to give them explicitly):

$$\bar{T}_{\text{av}} = \frac{T_0 + T_1}{C_{14}} + \frac{T_1 C_{21}}{C_{23}C_{34}} + \frac{T_2}{C_{23}C_{34}} + \frac{T_3}{C_{34}} \qquad \textbf{[S23]}$$

and

$$\bar{P}(S_0) = \left[1 + \frac{T_1 C_{21} C_{32}}{T_0 C_{10} C_{21} C_{32}} + \frac{T_2 C_{12} C_{32}}{T_0 C_{10} C_{21} C_{32}} + \frac{T_3 C_{12} C_{23}}{T_0 C_{10} C_{21} C_{32}} + \frac{T_4 C_{12} C_{23} C_{34}}{T_0 C_{10} C_{21} C_{32}}\right]^{-1}. \qquad \textbf{[S24]}$$

Table S2 shows that values calculated by the described method are in excellent agreement with the exact solution presented in *Formulation of the Hierachic Stochastic Model in Terms of Integral Equations* and the stochastic simulations presented in *Stochastic Simulations*, which confirms validity of the assumption made by Eq. **S21**.

Stochastic Simulations. In the last sections we have derived analytical expressions for statistical properties of Ca^{2+} spiking by means of the hierarchic stochastic model. However, the temporal evolution of the configurations $S_i(t)$, which illustrates the actual spiking pattern, needs to be resolved with a stochastic simulation algorithm. Such an algorithm is also required for the determination of statistic properties of model systems larger than the tetrahedron model. Larger models cannot be represented by linear chains, so that the expressions obtained in the last section are not applicable, and the full problem considered in *Formulation of the Hierachic Stochastic Model in Terms of Integral Equations* becomes too large for available numerical methods.

Delayed Stochastic Simulation Algorithm (DSSA). Because our problem is non-Markovian, waiting times between successive events are not exponentially distributed, and the standard method from Gillespie (12) cannot be applied. Therefore, we developed a DSSA, which is similar to those investigated in (13–15). However, unlike them, we do not draw random numbers from the waiting time distributions in advance to determine the transition times. Instead of that, we integrate stepwise over the distributions until the obtained value exceeds a random number drawn from the unit interval. The time is reset when a transition occurs. The full DSSA algorithm can be given in pseudocode as follows:

Data: initial cluster states x_j; transition probabilities $\psi(c_j, t - \tau x_j)$; transition types $\nu(x_j)$; total simulation time T; time step h.
Result: dynamics of the cluster states x_j.
begin
  generate $\{U_k\}_{k=1\ldots N_{\text{cl}}}$ as $U(0,1)$ random variables
  $\tau = 0$; $\{P_k\}_{k=1\ldots N_{\text{cl}}=0}$
  while $t < T$ do
    for $(j = 1; j <= N_{\text{cl}}; j++)$ do
      if $U_j > P_j$:
        $P_j += \int_{t-\tau}^{t-\tau+h} \psi(c_j, t', x_j)dt'$
      else:
        $x_j = x_j + \nu(x_j)$
        generate $\{U_k\}_{k=1\ldots N_{\text{cl}}}$ as $U(0,1)$ random variables
        $\tau = t$; $\{P_k\}_{k=1\ldots N_{\text{cl}}=0}$
        break
    $t = t + h$
end

In the above notation, "$U(0,1)$ random variables" means random numbers drawn from a uniform distribution in the interval (0, 1). In our case, the type of the transition $\nu(x_j)$ is uniquely determined for each state (open if closed and close if open),

and therefore the $\psi(c_j,t-\tau,x_j)$ are either ψ_o or ψ_c as defined in the main text, depending on x_j. In general, we would need a second random number to decide over the transition type, analogously to the original stochastic simulation algorithm from Gillespie (12).

Typical simulations are shown in Fig. 2 and Fig. S3. The tetrahedron model and the cube model both reproduce spike sequences similar to experimental data for the same set of parameters (Fig. S3). Ca^{2+} spikes (most clusters open) emerge from basal puff-activity (one cluster open) at irregular intervals. Long-term simulations ($\approx 10^6$ s) are used to compute spike statistics and are in excellent agreement with the analytic solutions (Table S2).

Efficiency of the DSSA for different model subtypes. The DSSA is particularly efficient if the integral of $\psi(c_j,t-\tau,x_j)$ in the above notation of the pseudocode is an analytic function. Then, at every time step, instead of applying a subroutine for numerical quadrature, we only need to compute the value of the survival function

$$\Psi(c_j,t-\tau,x_j) = 1 - \int_\tau^t \psi(c_j,t',x_j)dt', \qquad \textbf{[S25]}$$

which gives us the probability that the present configuration survives until time t. We thus only need to check if $U_j > \Psi(c_j,t-\tau,x_j)$; i.e., if the state survives even longer.

Integrals of the γ-distributions we use for the opening transitions (Ca^{2+} *Diffusion and Opening Transition Times*) are incomplete Euler Γ functions and integrals of exponentials as employed for the closing transitions (Eq. **2** of the main text) are exponentials again. Therefore, the described DSSA is very efficient in our case, and we can compute 10^6 s of simulated time of the tetrahedron model in minutes on a standard personal computer. Parameter scans of the irregular cube model, such as shown in Fig. 4, can be performed in 1–2 d. Note that for the tetrahedron model, it is still faster to compute the direct solution from *Stationary Statistics and the Tetrahedron Model*.

Implementation of the Global Feedback. In the main text (Eq. **1**), we introduced the addition of a global feedback to the model, and we showed that such a feedback shifts both the slope and the intercept of the σ–T_{av} relation (Fig. 4). In the following, details of the implementation of that feedback will be provided.

In Ca^{2+} *Diffusion and Opening Transition Times*, we showed that in our analysis, the probability density for opening of the first cluster $\psi_o(c_0,t-\tau)$ can be modeled by an exponential distribution $\lambda\exp[-\lambda(t-\tau)]$, where the parameter λ is the puff rate (Table 1). As stated in the context of Eq. **1** in the main text, we apply a global feedback to this first opening probability by assuming a dependence of the puff rate on the time elapsed since the last global spike, $t-t_{sp}$. Further, in the case of $\psi_o(c_0,\cdot)$, the last state transition, which occurred at time τ, is always a transition from one to zero open clusters, so that we can identify τ with the time of the last puff, $\tau = t_p$, and $\psi_o(c_0,\cdot)$ depends on three different times: the actual time t, the time of the last puff t_p, and the time of the last spike t_{sp}. After these considerations, we easily derive

$$\begin{aligned}\psi_o(c_0,t,t_p,t_{sp}) &= \lambda(t-t_{sp})e^{-\int_{t_p}^{t}\lambda(t'-t_{sp})dt'} \\ &= \lambda_0(1-e^{-\xi(t-t_{sp})})e^{-\frac{\lambda_0}{\xi}[-e^{-\xi(t-t_{sp})}+e^{-\xi(t_p-t_{sp})}-\xi(t-t_p)]}.\end{aligned} \qquad \textbf{[S26]}$$

From Eq. **S26**, it is immediately clear that the formalism derived in *Formulation of the Hierachic Stochastic Model in Terms of Integral Equations* and *Stationary Statistics and the Tetrahedron Model* is not applicable anymore because, therein, it was a prerequisite that state transitions depend only on time differences between subsequent state transitions. That is also evident from a physical point of view: Remembrance of the last occurrence of a specific configuration is far stronger non-Markovian than just remembrance of the time of the last configuration change.

But for such reasons, we developed the DSSA introduced in the last section and tested it against the analytic solutions for suitable test cases (Table S2). Indeed, our DSSA is particularly useful for applications such as Eq. **S26** because, rather than ψ_o, we need the survival probability Ψ_o given by Eq. **S25** in our algorithm:

$$\begin{aligned}\Psi_o(c_0,t,t_p,t_{sp}) &= 1 - \int_{t_p}^{t}\psi_o(c_0,t',t_p,t_{sp})dt' \\ &= e^{-\frac{\lambda_0}{\xi}(e^{-\xi(t-t_{sp})}-e^{-\xi(t_p-t_{sp})}+\xi(t-t_p))}.\end{aligned} \qquad \textbf{[S27]}$$

Therefore, the only change to the pseudocode provided in *Stochastic Simulations* is that we remember the occurrence of the last spike in order to compute the expression given above.

The σ–T_{av} Relation and Biological Function. Ca^{2+} signaling uses a variety of modes of information transmission (16–19). Frequency encoding is the mode that is relevant in the context here. How can stochastic sequences comply with this function of the pathway? What determines the information content of a random sequence of spikes, and how should ISI distributions respond to a stimulus?

The information content of a given ISI sequence can be determined by comparing it in a statistical sense with the "most random" sequence; i.e., with a pure Poisson process. That will tell us whether downstream parts of the pathway could in principle distinguish the given sequence from the most random sequence. The Kulback entropy of the given sequence relative to a Poisson process is a measure for the statistical difference. We calculated the Kulback entropy for spike sequences obeying linear σ–T_{av} relations in ref. 20. It depends essentially only on the slope m of that relation and is 0 for $m = 1$ (the given sequence would also be a pure Poisson process) and increases for decreasing m. We conclude that the slope of the σ–T_{av} relation is one of its properties, which is relevant for biological function.

ISI distributions should respond to a stimulus by moving to smaller average ISIs in order to obtain a change of the average frequency. The stimulated signal should also be detectable; i.e., there should be a typical frequency at which the spectrum of the stimulated ISI sequence should have a peak as sharp as possible. That requires a small standard deviation of the ISI sequences. A priori, a stochastic system with as many parameters as Ca^{2+} signaling could respond in different ways to stimulation, as sketched in Fig. S4. But only the response along the black arrow from large T_{av} and large σ to smaller T_{av} and small σ meets both requirements that T_{av} and σ decrease upon stimulation. Ca^{2+} signaling exhibits this response, and that warrants its biological function.

The response of Ca^{2+} signaling to stimulation described above does only live up to the requirements for a universal signaling mechanism if it is a property of the mechanism and not only of individual cells. Stimulation is, in mathematical terms, a change of parameter values. One way of guaranteeing a specific response of T_{av} and σ to parameter changes is the existence of a well-defined σ–T_{av} relation for the mechanism. If such a relation exists, changes of parameters only shift the position of the cell on the relation and do not move it to a position in the σ–T_{av} plane away from it. In experiments, the existence of such a relation means that all cells using the mechanism align along the relation, independent from their individual parameter values, and do not scatter all over the σ–T_{av} plane. It is also obvious that the most robust case, where changes of the values of all of the parameters do not move a cell away from the relation, will not exist in general. Changes of the values of some parameters will do so, and changes of the values of others will not.

Hence, the fact of the existence of a σ–T_{av} relation is important for pathway function. The experimental relations shown in ref. 21

are obtained by plotting the average and standard deviation from many different cells (population relation). The individual cells are different with respect to the value of many parameters like number of clusters, spatial cluster arrangement, concentrations of Ca^{2+}-binding proteins, volume, endoplasmic reticulum content, etc., but nonetheless they align along a linear function. We obtain the individual σ–T_{av} relation by conducting two or more different experiments with the same cell. We found agreement between the slope of the individual σ–T_{av} relation and the population relation (20, 21). Therefore, the experiments proved the existence of a σ–T_{av} relation.

Although the existence of the relation is not guaranteed in general, it might be a property of all spiking systems. That is not the case, however, as we could illustrate by calculations of σ and T_{av} for the perfect integrate and fire model, which is one of the prototypical spike-generating systems in neuronal membrane dynamics (22). Upon variation of parameters in that model, the data points occupy an area in the σ–T_{av} plane and do not align along a single curve as they do for the Ca^{2+} signaling model in Fig. 4 of the main text (with fixed global feedback). Consequently, there are spike-generating mechanisms that exhibit a σ–T_{av} relation, and there are mechanisms that do not.

In summary, the existence of a σ–T_{av} relation, the slope of the relation, and the fact that its course is from large σ and T_{av} to small σ and T_{av} are all relevant for the biological function of the pathway. The main text investigates the robustness of these properties.

1. Barton G (1989) *Elements of Green's Functions and Propagation: Potentials, Diffusion, and Waves* (Oxford Univ Press, London).
2. Higgins ER, Schmidle H, Falcke M (2009) Waiting time distributions for clusters of IP_3 receptors. *J Theor Biol* 259:338–349.
3. De Young GW, Keizer J (1992) A single-pool inositol 1,4,5-trisphosphate-receptor-based model for agonist-stimulated oscillations in Ca^{2+} concentration. *Proc Natl Acad Sci USA* 89:9895–9899.
4. Prager T, Falcke M, Schimansky-Geier L, Zaks MA (2007) Non-Markovian approach to globally coupled excitable systems. *Phys Rev E* 76:011118.
5. Van Kampen NG (2002) *Stochastic Processes in Physics and Chemistry*. (Elsevier Science, Amsterdam).
6. Cox D (1970) *Renewal Theory*. (Methuen, London).
7. Polyanin AD, Manzhirov AV (2008) *Handbook of Integral Equations*. (Chapman & Hall, London).
8. Wolkenfelt PHM (1981) The construction of reducible quadrature rules for Volterra integral and integro-differential equations. *IMA J Numeral Anal* 2:131–152.
9. Lubich CH (1983) On the stability of linear multistep methods for Volterra convolution equations. *IMA J Numer Anal* 3:439–465.
10. Heinrich R, Schuster S (1996) *The Regulation of Cellular Systems*. (Chapman & Hall, London).
11. Gillespie DT (1980) Transition time statistics in simple bi-stable chemical systems. *Physica A* 101:535–351.
12. Gillespie DT (1977) Exact stochastic simulation of coupled chemical reactions. *J Phys Chem* 81:2340–2361.
13. Bratsun D, Volfson D, Tsimring LS, Hasty J (2005) Delay-induced stochastic oscillations in gene regulation. *Proc Natl Acad Sci USA* 102:14593–14598.
14. Barrio M, Burrage K, Leier A, Tian T (2006) Oscillatory regulation of hes1: Discrete stochastic delay modelling and simulation. *PlOS Comput Biol* 2:1017–1030.
15. Schlicht R, Winkler G (2008) A delay stochastic process with applications in molecular biology. *J Math Biol* 57:613–648.
16. Larsen AZ, Olsen LF, Kummer U (2004) On the encoding and decoding of calcium signals in hepatocytes *Biophys Chem* 107:83–99.
17. Salazar C, Politi AZ, Hofer T (2008) Decoding of calcium oscillations by phosphorylation cycles: Analytic results. *Biophys J* 94:1203–1215.
18. Dolmetsch RE, Xu K, Lewis RS (1998) Calcium oscillations increase the efficiency and specificity of gene expression. *Nature* 392:933–936.
19. Zhu L, et al. (2008) Ca^{2+} oscillation frequency regulates agonist-stimulated gene expression in vascular endothelial cells*J Cell Sci* 121:2511–2518.
20. Skupin A, Falcke M (2007) Statistical properties and information content of calcium oscillations. *Genome Inform Ser* 18:44–53.
21. Skupin A, et al. (2008) How does intracellular Ca^{2+} oscillate: By chance or by the clock? *Biophys J* 94:2404–2411.
22. Skupin A, Falcke M (2009) From puffs to global Ca^{2+} signals: How molecular properties shape global signals *Chaos* 119:037111.
23. Smith IF, Parker I (2009) Imaging the quantal substructure of single IP_3R channel activity during Ca^{2+} puffs in intact mammalian cells. *Proc Natl Acad Sci USA* 106:6404–6409.
24. Skupin A, Falcke M (2010) Calcium signals driven by single channel noise. *PlOS Comput Biol* 6:e1000870.

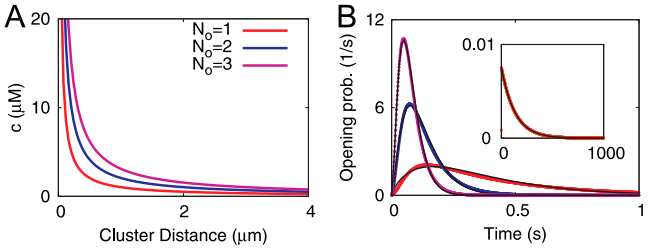

Fig. S1. Calculation of opening transition probabilities ψ_o. (*A*) The Ca^{2+} concentration at a closed cluster *c* depends on the distances to the open clusters. Shown is the diffusion profile as obtained from Eq. **S2** for the tetrahedron model (compare Fig. 2*A* in the main text), where all N_o open clusters have the same cluster distance. (*B*) Opening transition probabilities ψ_o for base-level $[Ca^{2+}]$ (*Inset*, orange) and for the $[Ca^{2+}]$ diffusion profiles depicted in *A* (the color-code is the same as in *A*). The transition probabilities were computed from the De Young–Keizer model with parameters given in Table S1, and were fitted (black lines) to exponential (*Inset*) and γ-distributions, as described in Ca^{2+} *Diffusion and Opening Transition Times*. The cluster distance is 1.5 μm. For parameter values not mentioned in this legend, see Table 1 of the main text.

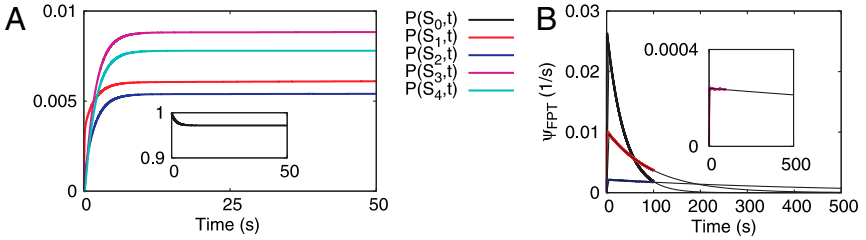

Fig. S2. Solution of the time-dependent analytic model. (*A*) The probabilities $P(S_i,t)$ attain stationarity after a few seconds. The probability that all clusters are closed, $P(S_0,t)$ (*Inset*), is highest. However, the probabilities for more open clusters also have probabilities different from zero, suggesting short spikes and longer time intervals in-between. The cluster distance is 1.5 μm , the decay rate is $\gamma = 15$ s^{-1}. (*B*) Calculation of ψ_{FPT}, σ, and T_{av} by integral equations. The colors indicate different values of the channel closing probability γ [black, 5 s^{-1}; red, 15 s^{-1}; blue, 25 s^{-1}; pink (*Inset*), 40 s^{-1}]. Average (T_{av}) and standard deviation (σ) of ISIs are the moments of the FPT distributions (see *Formulation of the Hierachic Stochastic Model in Terms of Integral Equations*). Because they have large nonzero tails, direct computation of the moments would require solution of the integral equations **S9** for >500 s, for which we have no efficient numerical procedures. Therefore, we fit the FPTs to the normalized, initially zero double exponential $\lambda_1\lambda_2/(\lambda_2-\lambda_1)\times(\exp[-\lambda_1 t]-\exp[-\lambda_2 t])$ (thin black lines). From these, we computed the values shown in Table S2. Parameters not mentioned in this legend are given in Table 1.

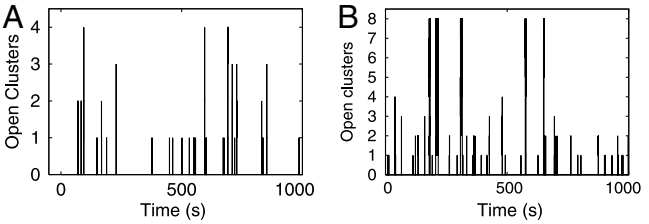

Fig. S3. Stochastic simulations. The tetrahedron model (*A*) and the cube model (*B*) show similar spike patterns with the same set of parameters (Table 1, $\gamma = 25$ s^{-1}). Calculations are performed with the DSSA described in *Stochastic Simulations*.

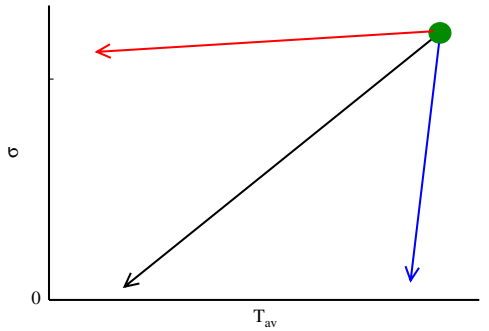

Fig. S4. Caricature of different responses of a cell to stimulation. Before stimulation, the cell has values of σ and T_{av}, as indicated by the green dot. The arrows indicate transitions to the values assumed upon stimulation. The red transition would provide for a change of the average ISI but would not decrease the standard deviation σ. The spectrum of that stimulated ISI sequence would be very broad, and the spike train would not have a typical frequency anymore. The blue transition would correspond to a typical frequency after stimulation but would not change the average ISI substantially. The black transition does change the average ISI and leads to a typical frequency. A response of the cell to stimulation along the black arrow corresponds to the σ–T_{av} relation of Ca^{2+} signaling and the requirements for frequency encoding.

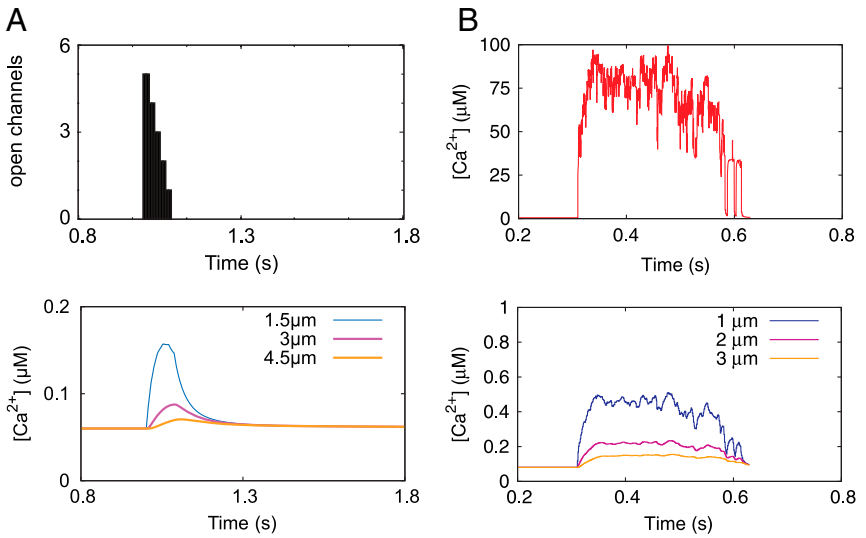

Fig. S5. Simulation of the rise of free $[Ca^{2+}]$ due to an open cluster. (*A*) The time course of channel closing was chosen according to the average measured rate in ref. 23. *Top*, number of open channels in the open cluster; *Bottom*, $[Ca^{2+}]$ at typical distances to neighbored clusters. (*B*) Simulation of a random and very long puff. *Top*, $[Ca^{2+}]$ at the open cluster; *Bottom*, $[Ca^{2+}]$ at typical distances to neighbored clusters. The simulations show that the assumption of a constant $[Ca^{2+}]$ at neighbored clusters during a puff is a good approximation, because the Ca^{2+} currents smooth out by diffusion, as referred to in *Methods* in the main text. We use linearized buffer and pump dynamics as described in ref. 24 with a total concentration of stationary buffer of 100 μM (dissociation constant 2 μM). Other parameter values are as follows: concentration of mobile buffer of 20 μM (*A*) and 100 μM (*B*) with dissociation constant 0.16 μM and diffusion coefficient 95 $\mu m^2 s^{-1}$; diffusion coefficient of free Ca^{2+} 220 $\mu m^2 s^{-1}$; pump flux coefficient 100 s^{-1}; 10 channels per cluster; single-channel current 0.12 pA (*A*) and 0.11 pA (*B*); cell radius 10 μm.

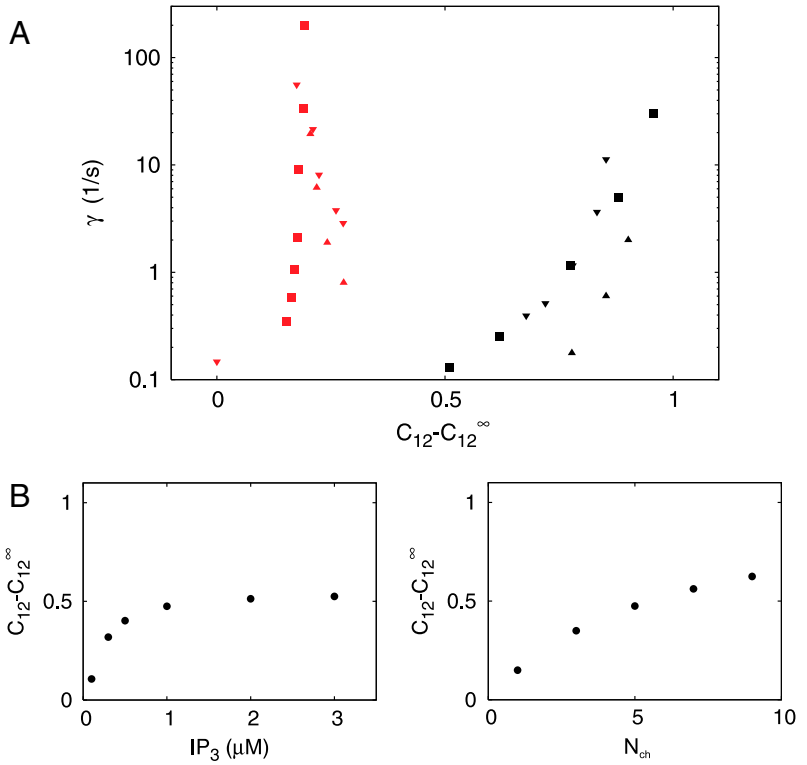

Fig. S6. Conditions for spiking. (*A*) Results of calculations analogous to those presented in Fig. 3*A* of the main text with variation of the number of channels per cluster N_{ch}. Spiking occurs for values of the coupling $C_{12} - C_{12}^{\infty}$ and the channel closing rate γ between the red and black symbols. We show here results for the four-cluster model with $N_{ch} = 3$ (upper triangles), $N_{ch} = 5$ (squares), and $N_{ch} = 9$ (lower triangles). Spiking is defined by a long-T_{av} criterion C_l (red) and a short-T_{av} criterion C_s (black), respectively. Coupling values smaller than C_l entail essentially only local puffs, and coupling values larger than C_s cause the regime of overstimulation. Each data point indicates the critical $(\gamma, C_{12} - C_{12}^{\infty})$ pair at a different cluster distance (values range from 0.5 μM to ∞) and the standard parameters (Table 1). The spike range increases with γ. (*B*) The cluster coupling $C_{12} - C_{12}^{\infty}$ depends on various system parameters like IP_3 concentration and N_{ch}.

Table S1. Parameter values for the De Young–Keizer model used to compute the opening transition times

Parameter	Value	Unit
a1	20	$(\mu M\,s)^{-1}$
a2	0.001	$(\mu M\,s)^{-1}$
a3	20	$(\mu M\,s)^{-1}$
a4	0.025	$(\mu M\,s)^{-1}$
a5	10	$(\mu M\,s)^{-1}$
d1	2.6	μM
d2	0.03077	μM
d3	2.6	μM
d4	0.1	μM
d5	12.25	μM

Table S2. Comparison of stationary values resulting from the different methods of computation described in *Formulation of the Hierachic Stochastic Model in Terms of Integral Equations*, *Stationary Statistics and the Tetrahedron Model*, and *Stochastic Simulations*

	Integral equations	Direct solution	DSSA
$\bar{P}(S_0)$	0.9719	0.9720	0.9715
$\bar{P}(S_4)$	0.0078	0.0078	0.0079
$\bar{T}_{av}$, s	98.39	98.44	98.68
$\bar{\sigma}$, s	98.07	98.11	98.68

The cluster distance is $a = 1.522$ μm; other parameters are given in Table 1